Neodymium-Doped Novel Barium Tungstate Nanospindles for the Enhanced Oxygen Evolution Reaction

Srinivasan Swathi, Marimuthu Priyanga, Yuvakkumar Rathinam,* Ravi Ganesan, Abdullah G. Al-Sehemi, and Dhayalan Velauthapillai*

Read Online

ACCESS | Metrics & More | Article Recommendations

ABSTRACT: In this work, pristine, 0.02, 0.04, and 0.06 M neodymium (Nd)-doped barium tungstate nanostructures were synthesized via a simple co-precipitation method for the water oxidation process. The obtained X-ray diffraction high-intensity peak at a 2θ value of 26.4° corresponding to the (112) lattice plane confirmed the formation of a tetragonal structure of $BaWO_4$. Moreover, the $BaWO_4$ morphology was examined by scanning electron microscopy, which showed the existence of nanospindles. An energy-dispersive X-ray spectrum confirmed the subsistence of the produced materials, for example, barium (Ba), tungsten (W), oxide (O), and neodymium (Nd), with weight percentages of 28.58, 46.63, 16.64, and 8.16%, respectively. The 0.04 M Nd-doped $BaWO_4$ product was explored to attain a high surface area of 18.18 m^2/g, a pore volume of 0.079 cm^3/g, and a pore diameter of 2.215 nm. Compared to the other prepared electrodes, the 0.04 M Nd-doped $BaWO_4$ product exhibited low overpotential values of 330 mV and 450 mV to deliver current densities of 10 mA/cm² and 50 mA/cm², respectively. In addition, the optimized electrode achieved a small Tafel slope value of 158 mV dec^{-1} and followed the Volmer−Heyrovsky mechanism. Moreover, the electrical conductivity of $BaWO_4$ was tuned due to the addition of a rare-earth metal dopant, and it exhibited the charge-transfer resistance and solution resistance values of 0.98 and 1.01 Ω, respectively. The prepared electrocatalyst was further studied by using cyclic voltammetry, and it exhibited a high double-layer capacitance value of 29.3 mF/cm² and high electrochemically active surface areas of 1.465 cm². The electrochemical performance was greatly improved depending on the concentration of the doping agent, and it was well consistent with the obtained results. The best electrocatalyst was subjected to a chronoamperometry test, which exhibited excellent stability even after 20 h. Hence, this work suggests that alkaline metal tungstates have a cost-effective, efficient, and promising electrocatalyst, and it is a new approach for the water oxidation process.
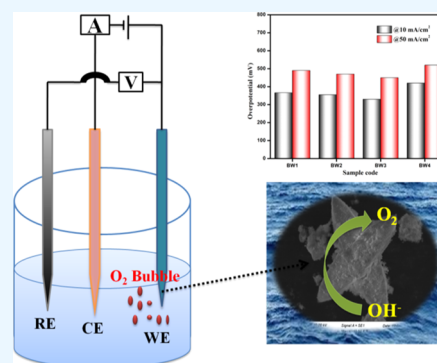
1. INTRODUCTION

The world's population has been enormously increasing due to which energy utilization has also been highly increasing and will continue to increase each century. In addition, exploitation of fossil fuels causes unavoidable environmental impacts, for example, climate changes, global warming, and so forth.[1,2] Recently, water splitting has gained much attention in energy conversion applications, and fossil fuels act a sustainable source of energy.[3] Numerous attempts have been made to prepare proficient, earth-abundant, and low-cost electrocatalysts for oxygen evolution reactions (OERs).[4] Notably, an OER is a four-electron reaction which needs high overpotential to deliver the appreciable current. Some important factors such as high surface area, excellent stability, and abundant active sites are still needed to improve the OER activity.[5] In both half-reactions, the catalytic performance was enhanced by using various benchmark materials such as Pt, RuO_2, IrO_2, and so forth[6] because such materials exhibited excellent performance including activity and durability. Nevertheless, it is not applicable for large-scale applications because of their high cost

and scarcity to use.[7] Accordingly, finding out earth-abundant, non-toxic, and economically suitable catalysts to possibly replace the high-cost materials for practical applications is required.[8] For the above multiple reasons, researchers have analyzed various materials such as non-metallic compounds, transition metal-based and alkaline metal-based oxides, molybdates, tungstates, sulfides, phosphides, nitrides, carbides, and so forth.[9−11] Among the various materials, metal tungstates have been used as attractive substances in wide applications because of their unique structural and magnetic properties to build superior electrocatalysts, which are employed in diverse applications such as humidity sensors, scintillators, and optical fibers.[12,13] Especially, rare-earth ion-
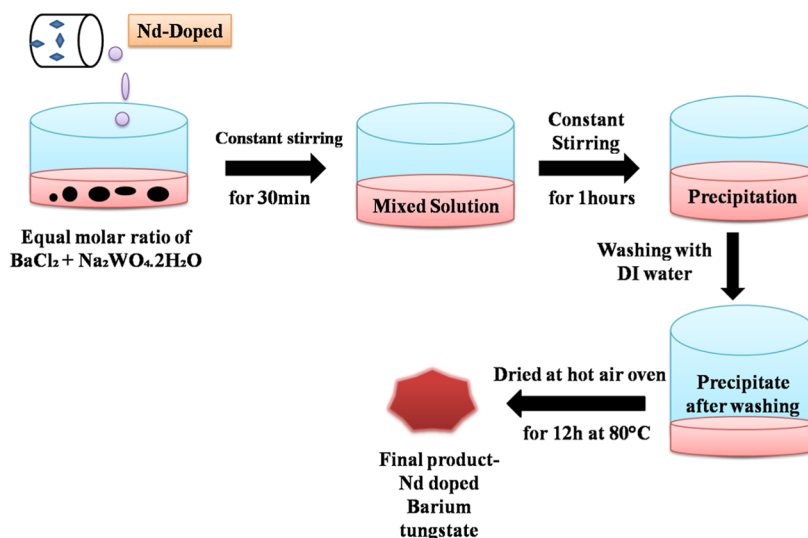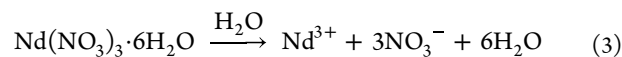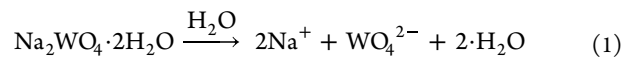
Figure 1. Schematic diagram of neodymium-doped barium tungstate nanostructures.

doped metal tungstates have superior thermal and chemical stability and have also been employed in various applications including solid-state lasers, white light-emitting diodes, solar cells, and so forth.[14] Numerous types of BaWO$_4$ morphologies have been obtained by choosing a suitable method. Various methods are performed to synthesize BaWO$_4$ nanostructures, such as hydrothermal/solvothermal, co-precipitation, solid-state reaction, polymeric precursor technique, cell electrochemical technique, molten salt technique, and microemulsion techniques.[15] However, co-precipitation is one of the simple and environment-friendly techniques to synthesize nanoparticles because of its simple reproducibility, low cost, elevated yield, and product purity.[16,17] It is suitable for the synthesis of BaWO$_4$ under easygoing conditions (i.e., ambient temperature and pressure). A BaWO$_4$ nanostructure has been analyzed by diverse applications as it is an attractive material in the electro-optic industry.[18] For example, Yu et al. synthesized samarium-doped Ba$_2$CaWO$_6$ phosphors via a solid-state process and studied their structural and optical properties. Moreover, they modified the synthesized materials through doping for LED applications.[19] Weng et al. synthesized tungsten oxide nanosheets via the hydrothermal process and fabricated barium bismuth niobate oxide layers on tungsten oxide nanosheets for photoelectrochemical water splitting. They achieved 6.02 mA/cm^2 at 1.23 V (vs RHE) by using the co-catalyst of Co$_{0.8}$Mn$_{0.2}$O$_x$ nanoparticles and exhibited excellent stability over 7 h.[20] Sundaresan et al. fabricated barium tungstate via a facile ultrasound-assisted method.[21] Pradeep et al. fabricated Tb^{3+}-doped barium tungstate thin films via pulsed laser deposition technique for photonic applications.[22] However, no studies have been found on the electrochemical OER, and it has been reported for the first time. In this work, pure and diverse doping concentrations (0.02, 0.04, and 0.06 M) of neodymium-doped barium tungstate nanostructures were successfully synthesized by using the simple co-precipitation process. The effects of rare-earth ion-doped barium tungstate nanostructures were examined by using various studies. The prepared electro-catalyst was tested using the electrochemical OER.

2. EXPERIMENTAL PROCEDURE

In the primary study, an equal molar ratio of barium chloride (BaCl$_2$) and sodium tungstate (Na$_2$WO$_4$) was dissolved in 50 mL of deionized water and subjected to magnetic stirring. A white precipitate was formed, which was filtered and cleaned using deionized water, ethanol, and methanol. The impurities in the above solution were eliminated and finally dried at 80 °C for 12 h (BW1). Likewise, three different 0.02, 0.04, and 0.06 M concentrations of neodymium (Nd) dopant samples were prepared. The three synthesized materials were termed as BW2, BW3, and BW4 and are shown in Figure 1.

BaWO$_4$ has been formed by the following chemical reaction

$$Na_2WO_4 \cdot 2H_2O \xrightarrow{H_2O} 2Na^+ + WO_4{}^{2-} + 2 \cdot H_2O \tag{1}$$

$$BaCl_2 \xrightarrow{H_2O} Ba^{2+} + 2Cl^- \tag{2}$$

$$Nd(NO_3)_3 \cdot 6H_2O \xrightarrow{H_2O} Nd^{3+} + 3NO_3{}^- + 6H_2O \tag{3}$$

At the final stage of the co-precipitation reaction at room temperature,

$$Ba^{2+} + WO_4{}^{2-} \xrightarrow{25\ °C} BaWO_4 \tag{4}$$

$$Ba^{2+} + Nd^{3+} + WO_4{}^{2-} \xrightarrow{25\ °C} (Ba,\ Nd)WO_4 \tag{5}$$
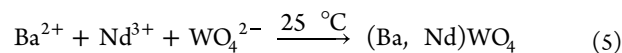
Then, the byproduct NaCl was excluded by the repetitive filtration process.[23]

The structure, morphology, elemental composition, and surface area of barium tungstate nanostructures were investigated using standard characterization. The electrochemical activity of the synthesized barium tungstate nanostructure products was measured by employing a Biologic SP-150 workstation. The electrochemical studies have been analyzed by using a Biologic SP-150 Potentiostat.

Linear sweep voltammetry (LSV) was performed using the SCE, which was converted to a RHE by using the Nernst equation. The Nernst equation is as follows: $E_{RHE} = E_{Ag/AgCl} + 0.197 + (0.059 \times pH)$, where E_{RHE} represents the reference RHE potential conversion, $E_{Ag/AgCl}$ represents the estimated potential relative to the reference (Ag/AgCl), 0.197 V

compared to the standard potential of Ag/AgCl (reference electrode), and the prepared electrolyte pH is 13.6. LSV was studied from 1.0 to 2.0 V versus RHE at a scan rate of 2 mV/s. Tafel slope plots were derived from LSV studies. Electrochemical impedance spectroscopy (EIS) measurements were studied from 100 kHz to 0.1 Hz at an amplitude of 5 mV. With the non-faradaic region, CV measurements were carried out from 0.2 to 0.3 V RHE at the different scan rates such as 10−100 mV/s. The double-layer capacitance (C_{dl}) values were calculated from CV curves, and the relation is as follows: $C_{dl} = \Delta j/2\nu$, where Δj represents the current density difference in the center potential values of CV curves and ν represents the scan rates. The electrochemically active surface area (ECSA) was estimated by using the relation ECSA = C_{dl}/C_s, where the value of C_s is 40 $\mu F/cm^2$, which is the general specific capacitance value of Ni foam.

3. RESULTS AND DISCUSSION

The X-ray diffraction (XRD) spectra of different concentrations of Nd-doped BaWO$_4$ nanostructures are shown in Figure 2. The obtained 2θ values of 17.0, 26.2, 27.9, 31.6, 42.9,
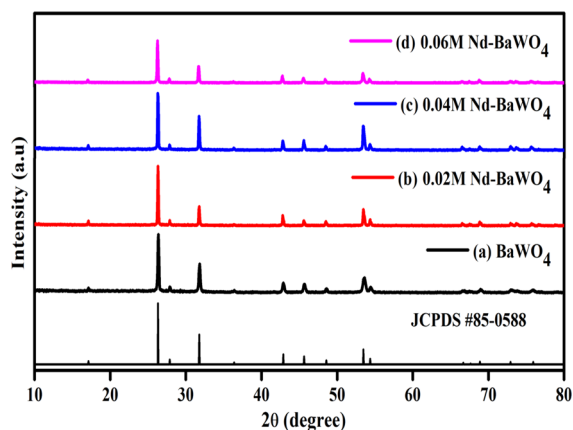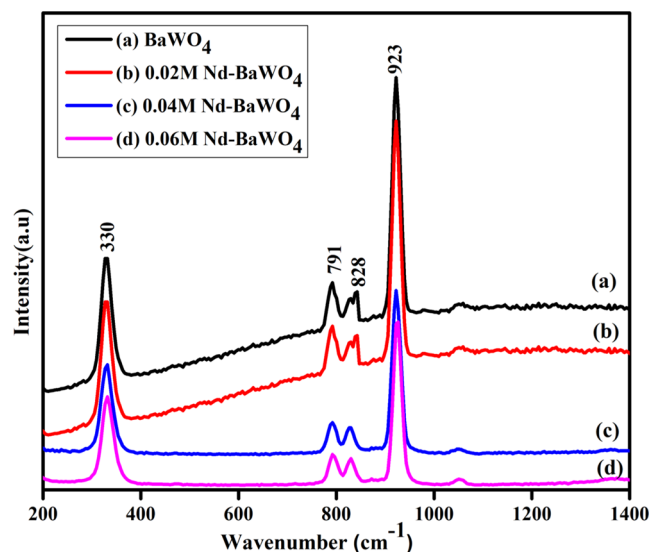
Figure 2. XRD spectra of (a) pure, (b) 0.02 M, (c) 0.04 M, and (d) 0.06 M Nd-doped barium tungstate nanostructures.

45.6, 48.6, 53.5, 54.3, 66.6, 67.4, 68.8, 72.9, 73.7, 75.7, 76.6, and 78.8° correspond to the (101), (112), (004), (200), (204), (220), (116), (312), (224), (402), (109), (235), (307), (404), (420), (334), and (111) lattice planes of barium tungstate. The sharp peak denotes the formation of a pure tetragonal unit cell structure of BaWO$_4$ with zero impurity phases. Furthermore, JCPDS card no. 85-0588 was coincident with the obtained results along with the lattice parameters ($a = 5.613$ and $c = 12.720$) and the $I4_1/a$ (88) space group.[24] The obtained XRD spectrum does not show any additional peaks; nevertheless, a slight displacement is acquired from its original position, which recommends the presence of the Nd dopant in BaWO$_4$. In addition, the peak's slight shift to a higher 2θ angle (toward right) confirms that Nd is effectively doped into the B-site of BaWO$_4$. Since the atomic radii of Nd is 0.182 nm, which is higher than that of W (0.139), nevertheless lesser than that of Ba (0.217 nm), as a result, Nd ions move to the W sites of BaWO$_4$. Generally, the host's lattice parameter and unit cell volume rise due to the larger atomic radii of the doping element, which was concluded with the XRD peaks' shift to higher angles.[25] The crystallite sizes of pure BaWO$_4$, 0.01 M Nd, and 0.02 M Nd-doped BaWO$_4$ product were estimated to

be 57.76, 57.75, 43.31, and 57.72 nm by employing $D = 0.9\lambda/\beta \cos\theta$.

Figure 3 shows the Raman spectra of Nd-doped BaWO$_4$ nanostructures. Five peaks were observed in Figure 3, which

Figure 3. Raman spectra of (a) pure, (b) 0.02 M, (c) 0.04 M, and (d) 0.06 M Nd-doped barium tungstate nanostructures.

were placed at wavenumbers of 330, 791, 828, and 923 cm^{-1} and viewed from 200 to 1400 cm^{-1}, respectively. The sharp peak at 923 cm^{-1} is attributed to the WO$_6$ symmetric stretching vibration of barium tungstate, whereas the other band situated at 330 cm^{-1} corresponds to the BaO$_6$ octahedra stretching vibration. After that, the other bands situated at 791 and 828 cm^{-1} correspond to the WO$_4$ tetrahedra stretching vibration.[26] In both XRD and Raman spectra, the peaks are slightly shifted toward the right due to substitutional doping. This may happen due to the decrease of particle size and the alteration in the bond length of the molecules. Moreover, it was well consistent with the obtained results and previous literature.[27]

Figure 4 shows the Fourier transform infrared (FTIR) spectra of Nd-doped BaWO$_4$ nanostructures. Seven distinct peaks were located from 4000 to 500 cm^{-1}. The main peak located at 810 cm^{-1} is attributed to metal oxide (M−O) vibrations such as Ba−O, W−O, and W−O−W stretching vibrations. Bands located at 3467, 2917, 2349, 1619, 1370, and 1107 cm^{-1} featured O−H and C−H bond symmetric and asymmetric vibrations, respectively.[28]

The morphologies of the synthesized materials such as pure (Figure 5a−c), 0.02 M (Figure 5d−f), 0.04 M (Figure 5g−i), and 0.06 M Nd-doped BaWO$_4$ (Figure 5j−l) nanostructures were investigated by using SEM and are shown in Figure 5a−l. The obtained SEM images clearly showed the flower-like structure, which was oriented together with numerous nanospindles. Nevertheless, in comparison to pure BaWO$_4$ (Figure 5a−c), rare-earth metal doping affects the size of BaWO$_4$, which facilitated more active sites to contribute in the electrocatalytic reaction.[29] The optimum amount of the doping agent tuned the morphology of the material, while the high concentration of the doping agent affects the morphology of the material. Since 0.06 M Nd-doped BaWO$_4$ exhibited the same nanospindle morphology, it appeared collapsed and agglomerated and exhibited a flower-like structure. The evaluated average particle size values of pure, 0.02, 0.04, and
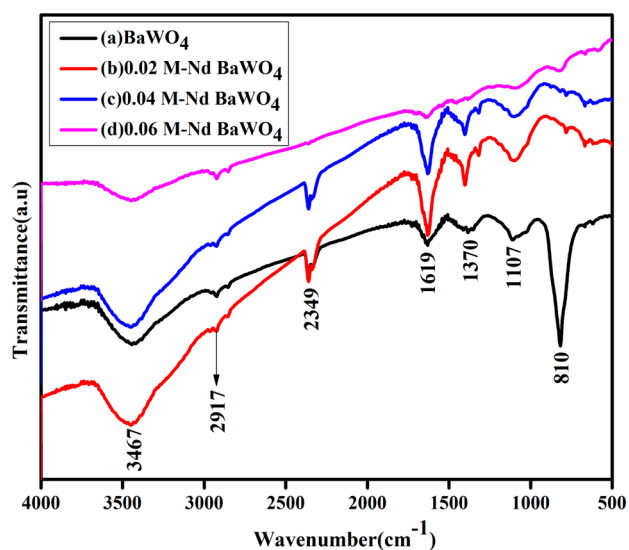
Figure 4. FTIR spectra of pure, 0.02, 0.04, and 0.06 M Nd-doped barium tungstate nanostructures.

0.06 M Nd-doped $BaWO_4$ are 484.3, 150.1, 142.4, and 327.2 nm, respectively, which were examined by employing Image J software. Among all the prepared samples, 0.04 M Nd-doped $BaWO_4$ exhibited low particle size, and as we expected, it displayed stronger catalytic performance than the other prepared materials. Then, it was further analyzed by the electrochemical studies.

Supported by the "Lewis acid−base" reaction, crystalline $BaWO_4$ was formed, which was synthesized by using the co-precipitation method. In this reaction, Ba^{2+} can accept a pair of electrons, while WO_4^{2-} can donate a pair of electrons. Then, the synthesized compound contains the formation of a coordination covalent bond ($Ba^{2+} \leftarrow :WO_4^{2-}$) between the Lewis acid and Lewis base.

The $BaWO_4$ growth is clearly shown in Figure 6. Initially, the primary nuclei of $BaWO_4$ were formed in the growth process. After that, the smaller nuclei were self-assembled, which led to the formation of an immature $BaWO_4$ structure. In the next stage, a large number of nuclei were assembled to form the intermediate nanostructure of $BaWO_4$. Finally, the growth was further increased to form the spindle-like $BaWO_4$ nanostructure. In this case, the rare-earth metal dopant reduces the particle size of the parent material. The bond energy
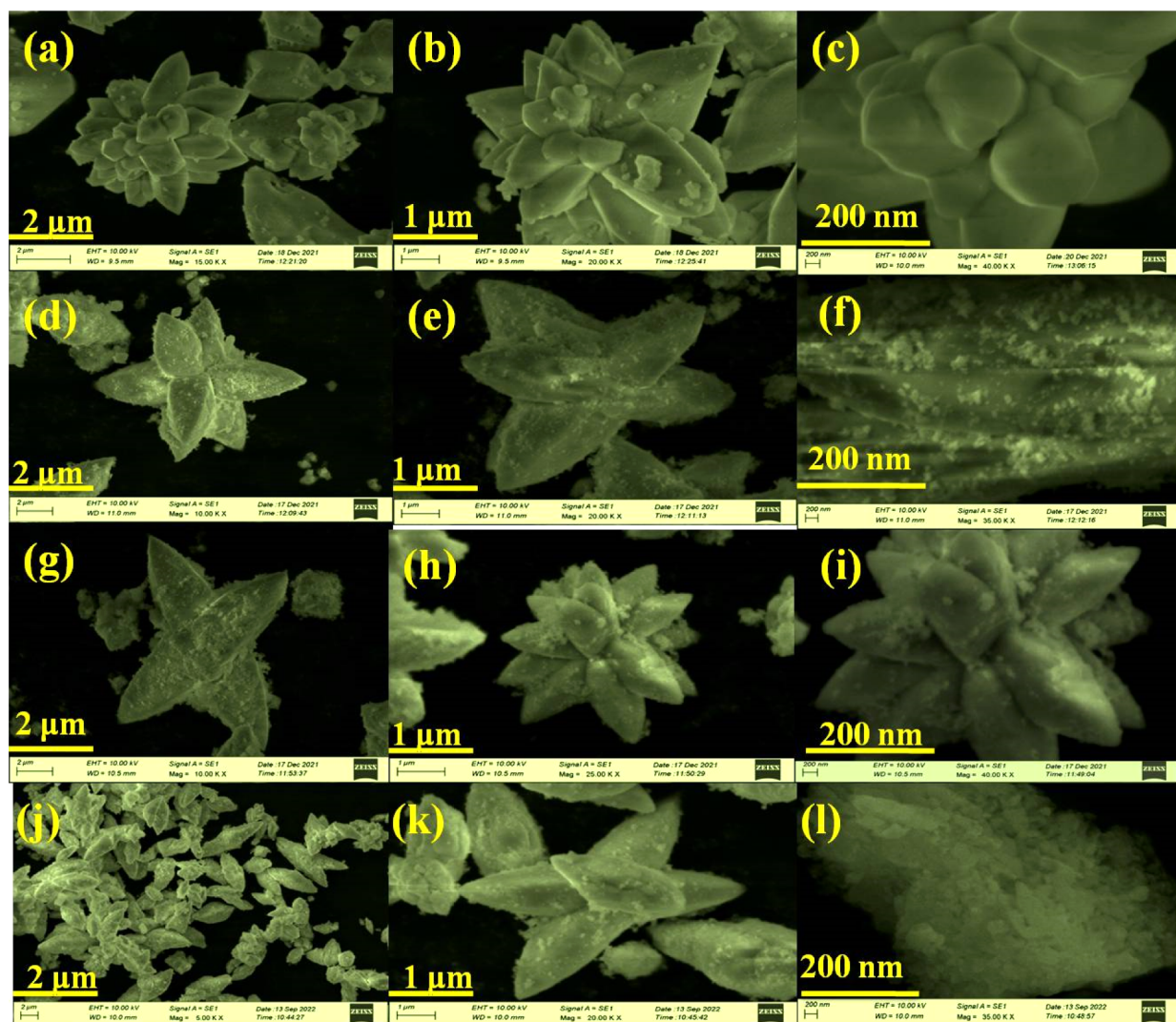
Figure 5. SEM images of (a−c) pure, (d−f) 0.02 M, (g−i) 0.04 M, and (j−l) 0.06 M Nd-doped barium tungstate nanostructures.
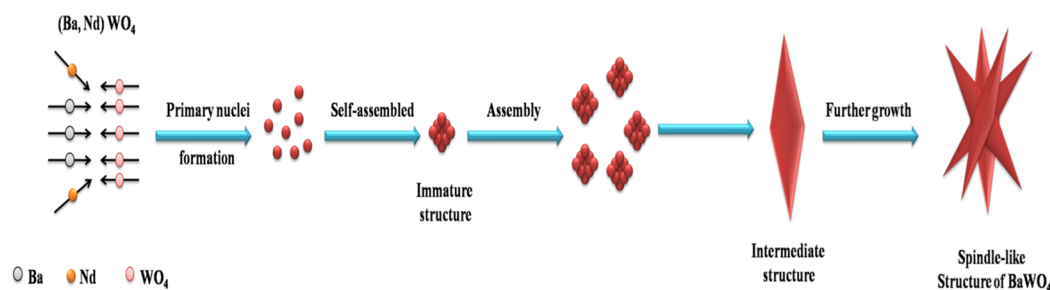
Figure 6. Growth mechanism of Nd-doped barium tungstate nanostructures.
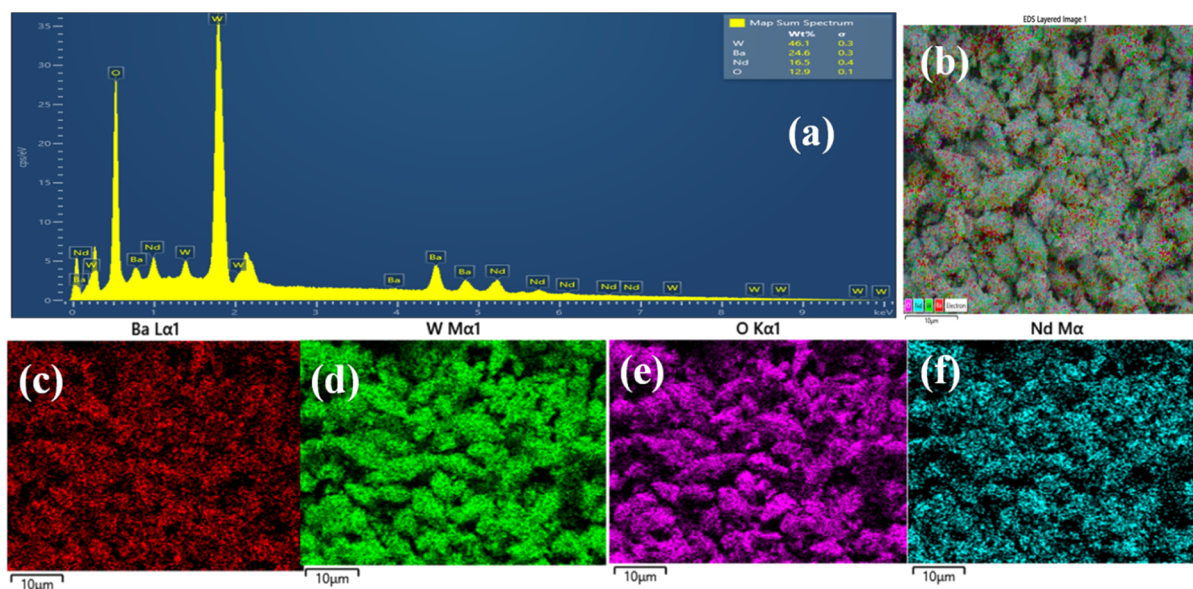
Figure 7. (a) EDX spectra and (b−f) EDX elemental mapping of 0.04 M Nd-doped barium tungstate nanostructures.

among rare-earth ions and tungstate ions is better than that among barium and tungstate ions.[23,29]

The energy-dispersive X-ray (EDX) spectra of the 0.04 M Nd-doped $BaWO_4$ nanostructure are shown in Figure 7a. This analysis confirmed the presence of barium (Ba), tungstate (W), oxide (O), and doping agent neodymium (Nd) in a suitable ratio without any existence of impurities. Moreover, the weight percentages of Ba, W, O, and Nd are 24.6, 46.1, 12.9, and 16.5%, respectively. Then, the purity of the sample was further confirmed with the EDX elemental mapping, which is shown in Figure 7b−f. It clearly shows that Ba, W, O, and Nd elements were uniformly distributed on the nanostructure. Therefore, this result suggests the purity of barium tungstate materials.

The surface composition and valance state of the dopant elements were exactly measured by using X-ray photoelectron spectroscopy (XPS) analysis (Figure 8a−e). The overall XPS survey spectrum clearly displays the existence of Ba, W, O, and Nd elements, which is shown in Figure 8a. The high-resolution XPS spectrum of Ba (Figure 8b) conveys the peak at binding energies 796.1 and 780.7 eV, which correlate with Ba $3d_{3/2}$ and Ba $5d_{5/2}$ and may be well attributed to the Ba^{2+} oxidation state, respectively. The high-resolution XPS spectrum of W (Figure 8c) expresses the peak at binding energies 38.4 and 36.3 eV, which correspond to W $4f_{5/2}$ and W $4f_{7/2}$ and may well be attributed to the W^{6+} oxidation state, respectively. The O 1s spectrum (Figure 8d) shows a peak at a binding energy of 531.3 eV, related to oxygen in $BaWO_4$. Figure 8e shows the peaks at binding energies 983.5 and 997 eV, related to Nd

$3d_{5/2}$ and Nd $3d_{3/2}$ and could be attributed to the Nd^{3+} oxidation state, respectively.[30]

The surface area of 0.04 M Nd-doped $BaWO_4$ nanostructures was analyzed with the help of BET analysis (Figure 9). The 0.04 M Nd-doped $BaWO_4$ nanostructures were explored to attain a surface area of 18.18 m^2/g, a pore volume of 0.079 cm^3/g, and a pore diameter of 2.215 nm. The prepared samples exhibited type IV isotherms because the hysteresis loop appeared within the range from 0.8 to 1.0 P/P_0. Furthermore, it indicated that the synthesized sample occurred with a mesoporous nature with a wide diameter. The elevated surface area and the quite porous structure of the prepared material provided a large number of catalytic active sites, leading to an increase in electrochemical activity.[31]

The electrochemical properties of the synthesized materials such as pure, 0.02, 0.04, and 0.06 M Nd-doped $BaWO_4$ nanostructures were analyzed. The electrocatalytic properties of all the prepared nanomaterials were examined by employing LSV. Figure 10a shows the LSV results of pure, 0.02, 0.04, and 0.06 M Nd-doped $BaWO_4$, which was measured in −0.2 to 1 V at 2 mV/s. The 0.04 M Nd-doped $BaWO_4$ nanostructure shows better activity with overpotential values of 330 and 450 mV at 10 and 50 mA/cm^2, lower than the rest of other electrocatalysts such as pure $BaWO_4$ (366 mV@10 mA/cm^2 and 490 mV@50 mA/cm^2), 0.02 M Nd-doped $BaWO_4$ (355 mV@10 mA/cm^2 and 470 mV@50 mA/cm^2), and 0.06 M Nd-doped $BaWO_4$ (420 mV@10 mA/cm^2 and 520 mV@50 mA/cm^2). The obtained result suggests that the electrochemical
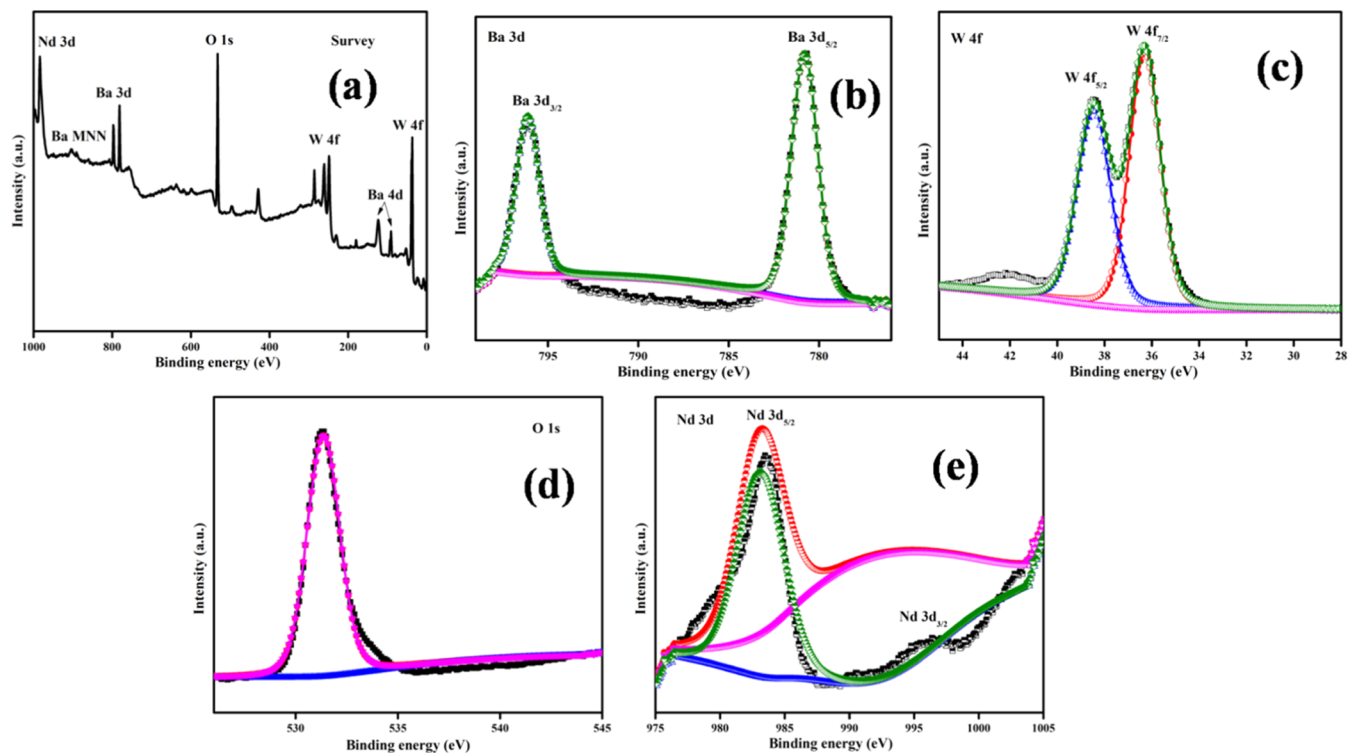
Figure 8. XPS spectra: (a) survey spectra and (b) Ba 3d, (c) W 4f, (d) O 1s, and (e) Nd 3d spectra of 0.04 M Nd-doped barium tungstate nanostructures.
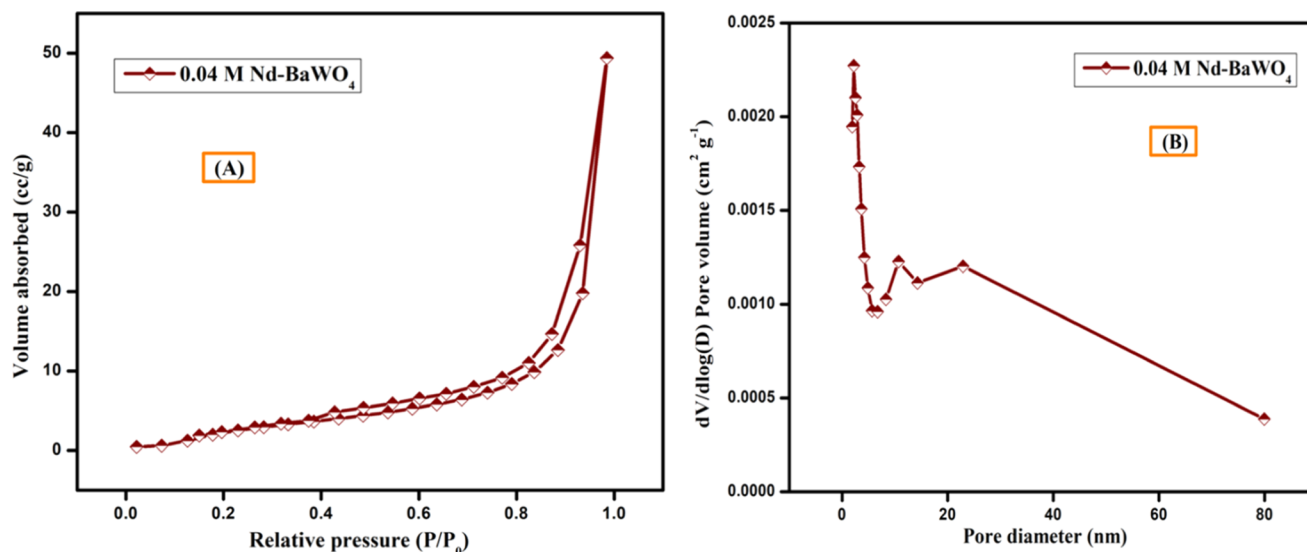

Figure 9. (A) Multi-point BET and (B) Barrett−Joyner−Halenda studies of 0.04 M Nd-doped barium tungstate nanostructures.

OER activity may be improved due to the addition of an optimum concentration of the rare-earth metal dopant Nd. An optimum amount of rare-earth dopant enhances the surface area of the material, which offers more catalytic active sites and enhanced OER activity (Table 1).[32]

The intrinsic catalytic activity of the synthesized material was examined by using the Tafel slope obtained from LSV (Figure 10c). The Tafel equation is $\eta = a + b \log j$. The Tafel slope value of 0.04 M Nd-doped $BaWO_4$ is 158 mV dec^{-1}, as low as that of pure $BaWO_4$ (178 mV dec^{-1}), 0.02 M Nd-doped $BaWO_4$ (172 mV dec^{-1}), and 0.06 M Nd-doped $BaWO_4$ (202 mV dec^{-1}). In an alkaline HER mechanism, three reaction

steps existed. They are Volmer ($H_2O + e^- \rightarrow H_{ads} + OH^-$; ~120 mV dec^{-1}), Heyrovsky ($H_2O + e^- + H_{ads} \rightarrow H_2 + OH^-$; 40 mV dec^{-1}), and Tafel ($H_{ads} + H_{ads} \rightarrow H_2$; 30 mV dec^{-1}), where H_{ads} represents the H_2 atom absorbed on the active sites of the synthesized material. The Tafel slope value of 0.04 M Nd-doped $BaWO_4$ is 158 mV dec^{-1}, which indicates that the 0.04 M Nd-doped $BaWO_4$ electrocatalyst follows a Volmer− Heyrovsky mechanism. The low overpotential and Tafel slope values of 0.04 M Nd-doped $BaWO_4$ recommended the favorable catalytic OER process.

EIS was employed to study the prepared electrode material kinetics. Figure 10d shows the EIS Nyquist plots of pure, 0.02,
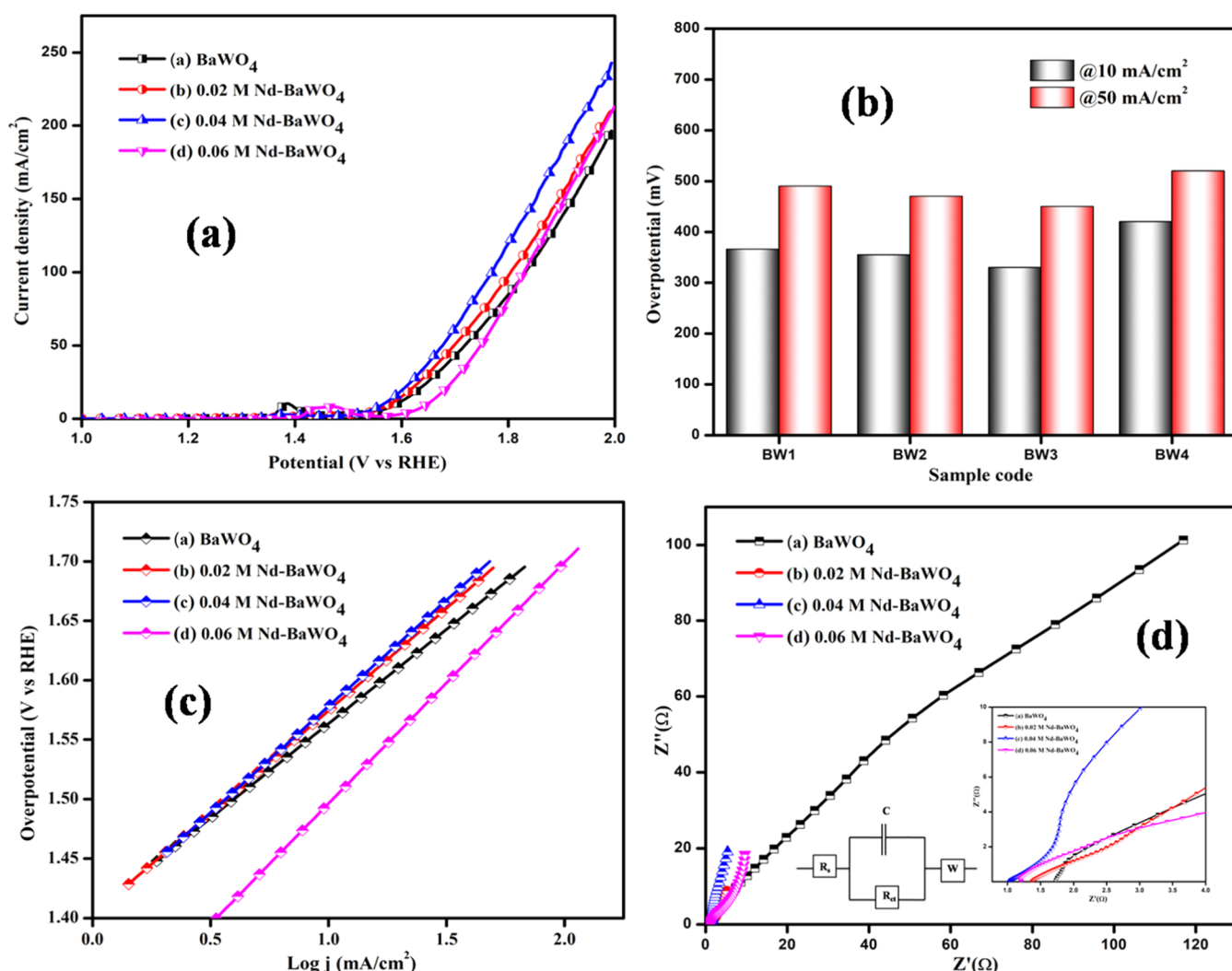
Figure 10. (a) LSV curves, (b) bar diagram, (c) Tafel slope, (d) EIS spectra of pure, 0.02, 0.04, and 0.06 M Nd-doped barium tungstate nanostructures.

Table 1. Comparison of the Prepared Electrocatalysts with Previous Metal Tungstates

electrocatalysts	overpotential (mV)@10 mA/cm^2	references
$Co_{0.5}Mn_{0.5}WO_4$	400	33
$NiWO_4$/Ni	363	34
$CoWO_4$/Ni	336	34
$FeWO_4$	459	35
$CuWO_4$	570	36
$CoWO_4$	383	35
$BaWO_4$	366	this work
0.04 M Nd-$BaWO_4$	330	this work

0.04, and 0.06 M Nd-doped $BaWO_4$ nanostructures. Commonly, EIS spectra consist of two half-regions. In brief, the first half-region has a semicircle, which was observed at a higher frequency region, and the other half-region has a slope line, which was observed at a low-frequency region.[37] The EIS measurement exhibited a low charge-transfer resistance value of 0.98 Ω for 0.04 M Nd-doped $BaWO_4$, denoting the fast electrode kinetics on the 0.04 M Nd-doped $BaWO_4$ electrocatalyst. In general, the charge transport kinetics linked with the charge transport resistance; similarly, the low charger-transfer resistances suggest the further favorable charge

transport kinetics.[38−40] The charge-transfer resistance values for the rest of the materials such as pure, 0.02 M, and 0.06 M Nd-doped $BaWO_4$ are 8.38, 2.48, and 1.69 Ω, respectively. Furthermore, the solution resistance values of pure, 0.02, 0.04, and 0.06 M Nd-doped $BaWO_4$ are 1.72, 1.36, 1.01, and 1.20 Ω, respectively. Then, an equivalent circuit was inserted as shown in Figure 9d, which consists of solution resistance (R_s), charge-transfer resistance (R_{ct}), capacitance (C), and Warburg impedance (W). Hence, EIS measurements suggest that the prepared 0.04 M Nd-doped $BaWO_4$ nanostructures have superior OER kinetics, resulting in a better electrochemical water oxidation performance.

ECSA was used to examine the active sites of the prepared electrode materials in the HER process. The C_{dl} value was evaluated from CV curves. Then, CV curves were evaluated at different scan rates such as 10, 20, 30, 40, 50, 60, 70, 80, 90, and 100 mV/s (which are shown in variant colors) in 0.2−0.3 V versus RHE (Figure 11a−d). Commonly, ECSA was related to active site estimation which was also proportional to double-layer capacitance (C_{dl}). In comparison to the other prepared catalysts, 0.04 M Nd-doped $BaWO_4$ exhibited the maximum electroactive area, which was confirmed from the CV curves.[41] The estimated double-layer capacitance values of pure, 0.02, 0.04, and 0.06 M Nd-doped $BaWO_4$ are 7.56, 26.7, 29.3, and
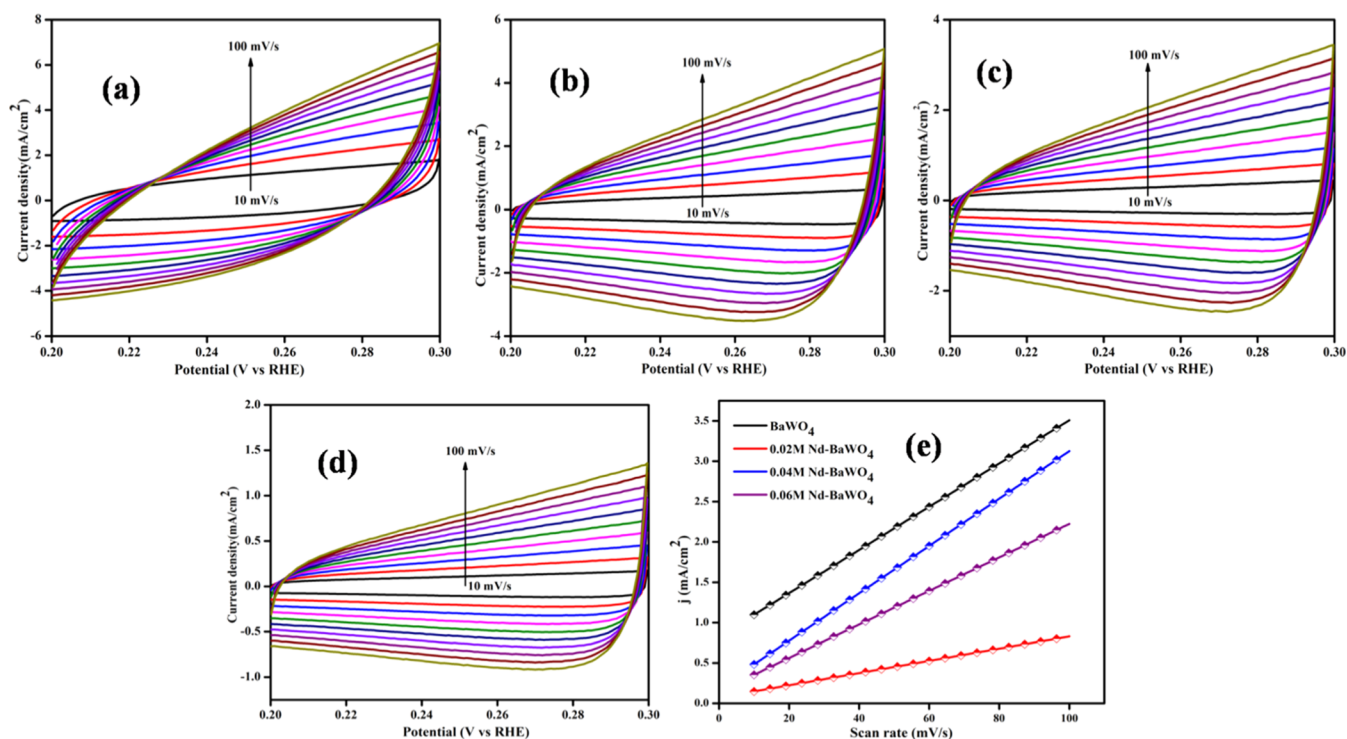
Figure 11. (a−d) CV curves and (e) double-layer capacitance of pure, 0.02, 0.04, and 0.06 M Nd-doped barium tungstate nanostructures.

20.7 mF/cm^2, respectively (Figure 11e). Furthermore, the ECSA values of pure, 0.02, 0.04, and 0.06 M Nd-doped BaWO$_4$ are 0.378, 1.335, 1.465, and 1.035 cm^2, respectively. The 0.04 M Nd-doped BaWO$_4$ nanostructure exhibited a high C_{dl} value than the other two electrocatalysts, suggesting that the high active sites existed in 0.04 M Nd-BaWO$_4$. Therefore, the high ECSA value of the optimized electrocatalyst suggests the existence of a superior number of catalytic active sites.

Commonly, the water splitting performance was improved by attaining some of the factors such as small particle size, high surface area, and a large number of active sites. Moreover, these factors are capably tuned depending on the appropriate doping concentration. Since the semiconducting nature of the host was largely destroyed due to the high doping concentration, the low doping concentration does not affect the semiconducting nature of the host.[42,43] In a high Nd dopant, the particle size did not decrease and exhibited a low electroactive area with low active sites, which was confirmed with the XRD, SEM, and CV results. Then, the morphology also collapsed and exhibited an agglomerated nanospindle morphology, which was oriented to the previous literature. For example, Hamed Shekarchizade et al. fabricated Ti/SnO$_2$−Sb− Ni electrodes with different Ni, Sb doping levels via the dip-coating thermal pyrolysis procedure for OER activity.[44] They reported that the low doping concentration of Ni improved the overpotential and electrode service life, whereas the high doping concentration of Ni affected the morphology and decreased the service life of the electrode. Böhm et al. synthesized V(III)-doped nickel oxide-based nanocatalysts via a rapid aqueous oxidation method for electrochemical water splitting. They also reported that up to 50 at. % V doping exhibited a low ECSA and high particle size and affects the nanosheet morphology, which could reduce the electro-chemical performance.[45] Hence, we expected to synthesize BaWO$_4$ nanostructures with an optimum amount of the Nd

dopant; as a result, it offered rich active sites and high conductivity.

In electrochemical water splitting, durability is an important criterion, which was used to assess the prepared material's stability. The prepared electrocatalyst of 0.04 M Nd-doped BaWO$_4$ was subjected to a chronoamperometry test for 20 h (Figure 12). Moreover, the 0.04 M Nd-doped BaWO$_4$
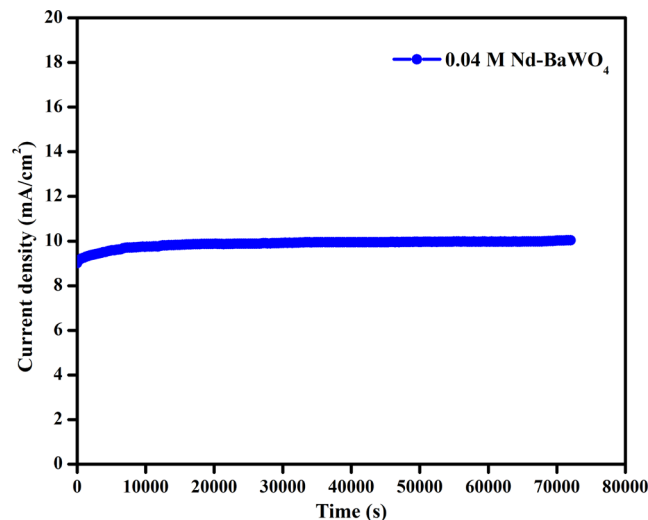
Figure 12. Chronoamperometry test for 0.04 M Nd-doped barium tungstate nanostructures.

nanostructure displayed an outstanding stability at 10 mA/ cm^2 for 20 h, which was clearly demonstrated with the obtained results. Therefore, the result suggests that the prepared electrocatalyst exhibits a superior performance for the electrochemical OER.

4. CONCLUSIONS

We effectively prepared pure, 0.02, 0.04, and 0.06 M Nd-doped $BaWO_4$ via a co-precipitation method for the electrochemical OER. Among all the prepared materials, 0.04 M Nd-doped $BaWO_4$ exhibited superb catalytic action with low over-potential and Tafel slope values of 330 mV and 158 mV dec^{-1}, respectively. Moreover, the Tafel slope values were reduced, and OER activities were improved with the increase in the concentration of rare-earth metal dopant (Nd). In addition, the low charge-transfer resistance (1.01 Ω) of 0.04 M Nd-doped $BaWO_4$ suggests quicker charge transport kinetics and also exhibited a surface area of 18.18 m^2/g. When the Nd concentration is lower than 0.06 M, it exhibits excellent OER activity with low overpotential and Tafel slope, which was confirmed with the obtained results. Likewise, 0.04 M Nd-doped $BaWO_4$ attained a high ECSA value of 1.465 cm^2, while 0.06 M Nd-doped $BaWO_4$ attained an ECSA value of only 1.035 cm^2, which could clearly suggest that the active site was high in 0.04 M Nd-doped $BaWO_4$. Therefore, the synergetic effect and more catalytic active sites of 0.04 M Nd-doped $BaWO_4$ exhibited excellent performance in OER.

■ AUTHOR INFORMATION

Corresponding Authors

Yuvakkumar Rathinam − *Department of Physics, Alagappa University, Karaikudi, Tamil Nadu 630 003, India;* orcid.org/0000-0001-6779-3453; Email: yuvakkumarr@alagappauniversity.ac.in

Dhayalan Velauthapillai − *Faculty of Engineering and Science, Western Norway University of Applied Sciences, Bergen 5063, Norway;* orcid.org/0000-0002-4162-7446; Email: dhayalan.Velauthapillai@hvl.no

Authors

Srinivasan Swathi − *Department of Physics, Alagappa University, Karaikudi, Tamil Nadu 630 003, India*

Marimuthu Priyanga − *Department of Physics, Alagappa University, Karaikudi, Tamil Nadu 630 003, India*

Ravi Ganesan − *Department of Physics, Alagappa University, Karaikudi, Tamil Nadu 630 003, India; Adjunct Professor, Department of Physics, Chandigarh University, Mohali, Punjab 140 413, India*

Abdullah G. Al-Sehemi − *Department of Chemistry, King Khalid University, Abha 61413, Saudi Arabia;* orcid.org/0000-0002-6793-3038

Complete contact information is available at:
https://pubs.acs.org/10.1021/acsomega.2c05156

Notes

The authors declare no competing financial interest.

■ ACKNOWLEDGMENTS

■ REFERENCES

(1) Tee, S. Y.; Win, K. Y.; Teo, W. S.; Koh, L. D.; Liu, S.; Teng, C. P.; Han, M. Y. Recent progress in energy-driven water splitting. *Adv. Sci.* **2017**, *4*, 1600337.

(2) Ahmed, J.; Alhokbany, N.; Ahamad, T.; Alshehri, S. M. Investigation of enhanced electro-catalytic HER/OER performances of copper tungsten oxide@ reduced graphene oxide nanocomposites in alkaline and acidic media. *New J. Chem.* **2022**, *46*, 1267.

(3) Joy, J.; Mathew, J.; George, S. C. Nanomaterials for photoelectrochemical water splitting−review. *Int. J. Hydrogen Energy* **2018**, *43*, 4804−4817.

(4) Ye, S.; Shi, W.; Liu, Y.; Li, D.; Yin, H.; Chi, H.; Luo, Y.; Ta, N.; Fan, F.; Wang, X.; Li, C. Unassisted photoelectrochemical cell with multimediator modulation for solar water splitting exceeding 4% solar-to-hydrogen efficiency. *J. Am. Chem. Soc.* **2021**, *143*, 12499−12508.

(5) Li, X.; Hao, X.; Abudula, A.; Guan, G. Nanostructured catalysts for electrochemical water splitting: current state and prospects. *J. Mater. Chem. A* **2016**, *4*, 11973−12000.

(6) Li, L.; Wang, P.; Shao, Q.; Huang, X. Metallic nanostructures with low dimensionality for electrochemical water splitting. *Chem. Soc. Rev.* **2020**, *49*, 3072−3106.

(7) Zhang, Y.; Wang, Q.; Zhu, K.; Ye, K.; Wang, G.; Cao, D.; Yan, J. Edge sites-driven accelerated kinetics in ultrafine Fe_2O_3 nanocrystals anchored graphene for enhanced alkali metal ion storage. *Chem. Eng. J.* **2022**, *428*, 131204.

(8) Geng, J. J.; Guo, S.; Zhang, Z. C.; Guo, H. B.; Xie, Y. P. Effect of tungsten/graphene/tungsten interface on helium diffusion kinetics and mechanical properties and defects of tungsten as first wall material-first principle calculation. *J. Alloys Compd.* **2021**, *851*, 156760.

(9) Zhao, T.; Ye, G.; Zhao, Z.; Ghahreman, A.; Sun, F.; Liu, X.; Lei, Y. A clean non-toxic method for leaching of barium tungstate. *Sep. Purif. Technol.* **2022**, *282*, 120062.

(10) Piper, T.; Heimbach, S.; Adamczewski, M.; Thevis, M. An in vitro assay approach to investigate the potential impact of different doping agents on the steroid profile. *Drug Test. Anal.* **2021**, *13*, 916−928.

(11) Ali, M.; Pervaiz, E.; Rabi, O. Enhancing the Overall Electrocatalytic Water-Splitting Efficiency of Mo_2C Nanoparticles by Forming Hybrids with UiO-66 MOF. *ACS Omega* **2021**, *6*, 34219−34228.

(12) Yan, Q.; Cai, Z. Issues in preparation of metal-lignin nanocomposites by coprecipitation method. *J. Inorg. Organomet. Polym. Mater.* **2021**, *31*, 978−996.

(13) Patiño-Ruiz, D. A.; Meramo-Hurtado, S. I.; González-Delgado, Á.D.; Herrera, A. Environmental sustainability evaluation of iron oxide nanoparticles synthesized via green synthesis and the coprecipitation method: A comparative life cycle assessment study. *ACS Omega* **2021**, *6*, 12410−12423.

(14) Bondarenko, G. G.; Fisher, M. R.; Kristya, V. I.; Bondariev, V. A. Modeling of thermofield electron emission from the cathode with a thin insulating film on the surface in gas discharge plasma. *High Temp. Mater. Processes* **2022**, *26*, 17.

(15) Li, J.; Wei, J.; Feng, Y.; Li, X. Effect of CaO on phase composition and properties of aluminates for barium tungsten cathode. *Materials* **2018**, *11*, 1380.

(16) Wang, R.; Cao, Z.; Wei, L.; Bai, L.; Wang, H.; Zhou, S.; Zhan, S.; Ji, B.; Li, Z.; Gao, S.; Xie, J.; Ma, Q. Barium tungstate nanoparticles to enhance radiation therapy against cancer. *Nanomedicine* **2020**, *28*, 102230.

(17) Muthukutty, B.; Vivekanandan, A. K.; Chen, S. M.; Sivakumar, M.; Chen, S. H. Designing hybrid barium tungstate on functionalized carbon black as electrode modifier for low potential detection of antihistamine drug promethazine hydrochloride. *Composites, Part B* **2021**, *215*, 108789.

(18) Huang, Y.; Zhang, Q. Y.; Liao, Q.; Chen, Y.; Yan, X.; Guo, X. J.; Lang, W. Z. Influence of Cr doping on hydrogen permeation

performance of lanthanum tungstate membrane. *Sep. Purif. Technol.* **2021**, *262*, 118333.

(19) Yu, R.; Mi Noh, H. M.; Kee Moon, B. K.; Chun Choi, B. C.; Hyun Jeong, J. H.; Sueb Lee, H. S.; Jang, K.; Soo Yi, S. S. Photoluminescence characteristics of Sm_{3+}-doped Ba_2CaWO_6 as new orange−red emitting phosphors. *J. Lumin.* **2014**, *152*, 133−137.

(20) Weng, B.; Grice, C. R.; Ge, J.; Poudel, T.; Deng, X.; Yan, Y. Barium Bismuth Niobate Double Perovskite/Tungsten Oxide Nanosheet Photoanode for High-Performance Photoelectrochemical Water Splitting. *Adv. Energy Mater.* **2018**, *8*, 1701655.

(21) Sundaresan, P.; Lee, C. H.; Fu, C. C.; Liu, S. H.; Juang, R. S. Ultrasound-assisted synthesis of barium tungstate encapsulated carbon nanofiber composite for real-time sensing of p-cresol in human urine samples. *Microchem. J.* **2021**, *166*, 106239.

(22) Pradeep, S. G.; Sreedharan, R. S.; Suresh, S.; Kavitha, V. S.; Venugopala Pillai, N. V.; Mahadevan Pillai, V. M. Luminescent Tb_{3+} doped barium tungstate thin films as a potential candidate for photonic applications. *J. Lumin.* **2020**, *226*, 117484.

(23) Jiang, G.; Kitani, S.; Kawaji, H. Synthesis and characterization of Na-containing amorphous and nanocrystalline Si from the reaction of NaSi with $AlCl_3$. *J. Non-Cryst. Solids* **2017**, *464*, 92−95.

(24) Nabi, G.; Ali, W.; Majid, A.; Alharbi, T.; Saeed, S.; Albedah, M. A. Controlled growth of Bi-Functional La doped CeO_2 nanorods for photocatalytic H_2 production and supercapacitor applications. *Int. J. Hydrogen Energy* **2022**, *47*, 15480.

(25) Song, Z.; Ma, J.; Li, X.; Sun, Y.; Fang, J.; Liu, Z.; Gao, C. Electrochemical synthesis and characterization of barium tungstate crystallites. *J. Am. Ceram. Soc.* **2009**, *92*, 1354−1357.

(26) Pillai, N. V.; Pillai, V. M.; Vinodkumar, R.; Navas, I.; Ganesan, V.; Koshy, P. Influence of europium oxide doping on the structural and optical properties of pulsed laser ablated barium tungstate thin films. *J. Alloys Compd.* **2011**, *509*, 2745−2752.

(27) Kumar, V.; Ahlawat, D. S.; AarifUl Islam, S. A.; Singh, A. Ce doping induced modifications in structural, electrical and magnetic behaviour of hematite nanoparticles. *Mater. Sci. Eng. B* **2021**, *272*, 115327.

(28) AlShehri, S. M.; Ahmed, J.; Ahamad, T.; Almaswari, B. M.; Khan, A. Efficient photodegradation of methylthioninium chloride dye in aqueous using barium tungstate nanoparticles. *J. Nanopart. Res.* **2017**, *19*, 289.

(29) AlShehri, S. M.; Ahmed, J.; Ahamad, T.; Almaswari, B. M.; Khan, A. Efficient photodegradation of methylthioninium chloride dye in aqueous using barium tungstate nanoparticles. *J. Nanopart. Res.* **2017**, *19*, 289.

(30) Luo, Z.; Li, H.; Xia, J.; Zhu, W.; Guo, J.; Zhang, B. Microwave-assisted synthesis of barium tungstate nanosheets and nanobelts by using polymer PVP micelle as templates. *Mater. Lett.* **2007**, *61*, 1845−1848.

(31) Karkera, G.; Sarkar, T.; Bharadwaj, M. D.; Prakash, A. S. Design and development of efficient bifunctional catalysts by tuning the electronic properties of cobalt−manganese tungstate for oxygen reduction and evolution reactions. *ChemCatChem* **2017**, *9*, 3681−3690.

(32) Srirapu, V. K. V. P.; Kumar, A.; Srivastava, P.; Singh, R. N.; Sinha, A. S. K. Nanosized $CoWO_4$ and $NiWO_4$ as efficient oxygen-evolving electrocatalysts. *Electrochim. Acta* **2016**, *209*, 75−84.

(33) Nakayama, M.; Takeda, A.; Maruyama, H.; Kumbhar, V.; Crosnier, O. Cobalt-substituted iron-based wolframite synthesized via polyol route for efficient oxygen evolution reaction. *Electrochem. Commun.* **2020**, *120*, 106834.

(34) Ahmed, J.; Ahamad, T.; Alhokbany, N.; Almaswari, B. M.; Ahmad, T.; Hussain, A.; Al-Farraj, E. S. S.; Alshehri, S. M. Molten salts derived copper tungstate nanoparticles as bifunctional electro-catalysts for electrolysis of water and supercapacitor applications. *ChemElectroChem* **2018**, *5*, 3938−3945.

(35) Zawawi, S. M. M.; Yahya, R.; Hassan, A.; Mahmud, H. N. M.; Daud, M. N. Structural and optical characterization of metal tungstates (MWO_4; M= Ni, Ba, Bi) synthesized by a sucrose-templated method. *Chem. Cent. J.* **2013**, *7*, 80.

(36) Zhang, Y.; Ni, Z.; Yao, J. Enhancement of the activity of electrochemical oxidation of BPS by Nd-doped PbO_2 electrodes: performance and mechanism. *Water* **2020**, *12*, 1317.

(37) Hong, D.; Yamada, Y.; Nomura, A.; Fukuzumi, S. Catalytic activity of $NiMnO_3$ for visible light-driven and electrochemical water oxidation. *Phys. Chem. Chem. Phys.* **2013**, *15*, 19125−19128.

(38) Majhi, K. C.; Yadav, M. Neodymium oxide doped neodymium phosphate as efficient electrocatalyst towards hydrogen evolution reaction in acidic medium. *J. Environ. Chem. Eng.* **2022**, *10*, 107416.

(39) Premathilake, D.; Outlaw, R. A.; Parler, S. G.; Butler, S. M.; Miller, J. R. Electric double layer capacitors for ac filtering made from vertically oriented graphene nanosheets on aluminum. *Carbon* **2017**, *111*, 231−237.

(40) Bo, Z.; Wen, Z.; Kim, H.; Lu, G.; Yu, K.; Chen, J. One-step fabrication and capacitive behavior of electrochemical double layer capacitor electrodes using vertically-oriented graphene directly grown on metal. *Carbon* **2012**, *50*, 4379−4387.

(41) Zhai, P.; Xia, M.; Wu, Y.; Zhang, G.; Gao, J.; Zhang, B.; Cao, S.; Zhang, Y.; Li, Z.; Fan, Z.; Wang, C.; Zhang, X.; Miller, J. T.; Sun, L.; Hou, J. Engineering single-atomic ruthenium catalytic sites on defective nickel-iron layered double hydroxide for overall water splitting. *Nat. Commun.* **2021**, *12*, 4587.

(42) Fominykh, K.; Chernev, P.; Zaharieva, I.; Sicklinger, J.; Stefanic, G.; Döblinger, M.; Müller, A.; Pokharel, A.; Böcklein, S.; Scheu, C.; Bein, T.; Fattakhova-Rohlfing, D. Iron-doped nickel oxide nanocrystals as highly efficient electrocatalysts for alkaline water splitting. *ACS Nano* **2015**, *9*, 5180−5188.

(43) Zhao, T.; Shen, X.; Wang, Y.; Hocking, R. K.; Li, Y.; Rong, C.; Dastafkan, K.; Su, Z.; Zhao, C. In situ reconstruction of V-doped Ni_2P pre-catalysts with tunable electronic structures for water oxidation. *Adv. Funct. Mater.* **2021**, *31*, 2100614.

(44) Shekarchizade, H.; Amini, M. K. Effect of elemental composition on the structure, electrochemical properties, and ozone production activity of Ti/SnO_2-Sb-Ni electrodes prepared by thermal pyrolysis method. *Int. J. Electrochem.* **2011**, *2011*, 240837.

(45) Böhm, D.; Beetz, M.; Kutz, C.; Zhang, S.; Scheu, C.; Bein, T.; Fattakhova-Rohlfing, D. V (III)-Doped Nickel Oxide-Based Nanocatalysts for Electrochemical Water Splitting: Influence of Phase, Composition, and Doping on the Electrocatalytic Activity. *Chem. Mater.* **2020**, *32*, 10394−10406.